nature communications

Article

https://doi.org/10.1038/s41467-024-55433-1

Magnetochiral charge pumping due to charge trapping and skin effect in chirality-induced spin selectivity

Received: 30 March 2023

Accepted: 12 December 2024

Published online: 02 January 2025

Check for updates

Yufei Zhao[1,4], Kai Zhang[2,4], Jiewen Xiao[1], Kai Sun[2] & Binghai Yan[1,3]

Chirality-induced spin selectivity (CISS) generates giant spin polarization in transport through chiral molecules, paving the way for novel spintronic devices and enantiomer separation. Unlike conventional transport, CISS magnetoresistance (MR) violates Onsager's reciprocal relation, exhibiting significant resistance changes when reversing electrode magnetization at zero bias. However, its underlying mechanism remains unresolved. In this work, we propose that CISS MR originates from charge trapping that modifies the electron tunneling barrier and circumvents Onsager's relation, distinct from previous spin polarization-based models. Charge trapping is governed by the non-Hermitian skin effect, where dissipation leads to exponential wavefunction localization at the ferromagnet-chiral molecule interface. Reversing magnetization or chirality alters the localization direction, changing the occupation of impurity/defect states in the molecule (*i.e.*, charge trapping) – a phenomenon we term magnetochiral charge pumping. Our theory explains why CISS MR can far exceed the ferromagnet spin polarization and why chiral molecules violate the reciprocal relation but chiral metals do not. Furthermore, it predicts exotic phenomena beyond the conventional CISS framework, including asymmetric MR induced by magnetic fields alone (without ferromagnetic electrodes), as confirmed by recent experiments. This work offers a deeper understanding of CISS and opens avenues for controlling electrostatic interactions in chemical and biological systems through the magnetochiral charge pumping.

Chirality is a fundamental concept in chemistry, physics, and biology[1]. Recently, chirality was reported to generate spin polarization that is far larger than an ordinary ferromagnet (FM), called chiral-induced spin selectivity (CISS)[2]. CISS opens exciting pathways to design unconventional spintronic devices using chiral molecules, perform chiral separation via magnetism, and explore the spin-selective biological process[3,4]. However, the physical mechanism underlying CISS is elusive and debated[5,6], although some spin polarization-based models[7–10] reflect some consistent features with experiments.

In experiments, CISS is commonly probed by a two-terminal magnetoresistance (MR)[11–18] where the chiral molecule is sandwiched between an FM electrode and a nonmagnetic lead (see Fig. 1d for illustration). The resistance changes by flipping the electrode magnetization (M). Because MR exhibits a feature similar to a magnetic tunneling junction, chiral molecules were usually presumed to induce spin

[1]Department of Condensed Matter Physics, Weizmann Institute of Science, Rehovot, Israel. [2]Department of Physics, University of Michigan, Ann Arbor, MI, USA. [3]Department of Physics, the Pennsylvania State University, University Park, PA, USA. [4]These authors contributed equally: Yufei Zhao, Kai Zhang.
e-mail: binghai.yan@weizmann.ac.il

https://doi.org/10.1038/s41467-024-55433-1

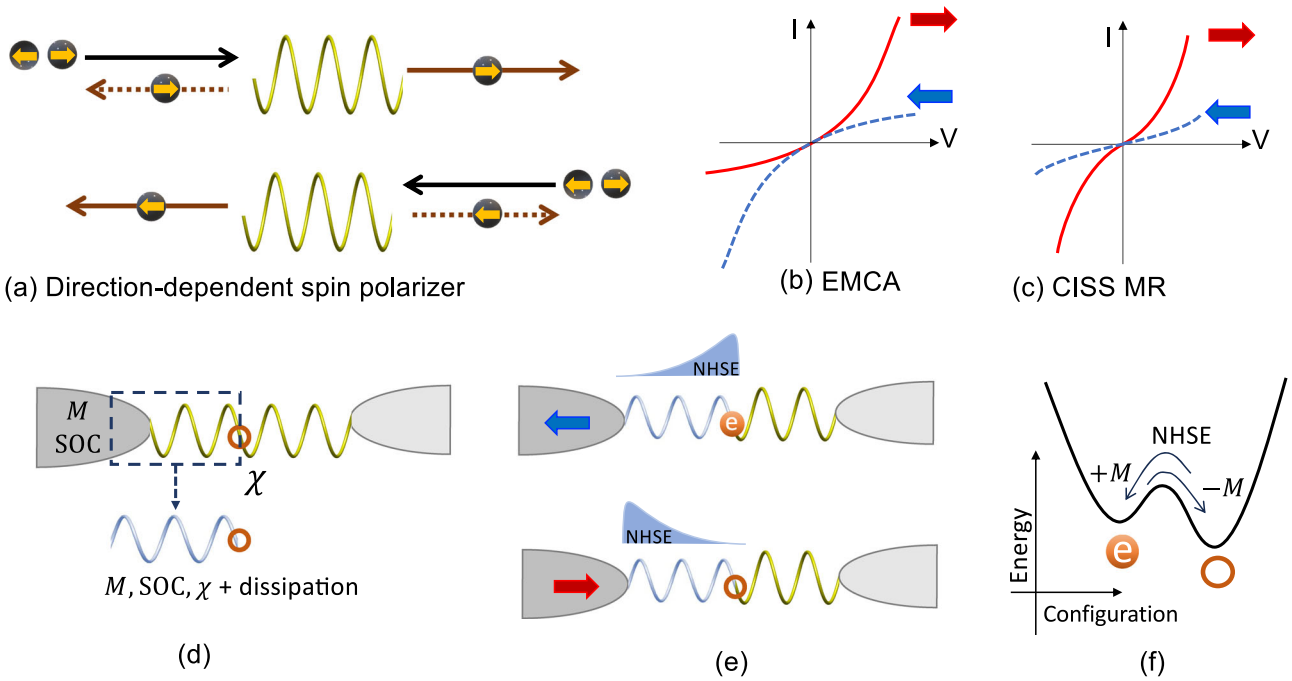

Fig. 1 | Chirality-driven magnetoresistance (MR) including the electrical magnetochiral anisotropy (EMCA) and chirality-induced spin selectivity (CISS). **a** Transmitted (solid line) and reflected (dashed line) electrons through a chiral molecule get spin-polarized (indicated by small yellow arrows) for unpolarized incident electrons. In a perturbative picture, because the spin polarization relies on the incident direction, the resistance is direction-dependent when the spin polarizer is connected to a ferromagnetic electrode (magnetization indicated by the red/blue arrows), leading to EMCA rather than CISS MR. **b**, **c** shows the typical I–V curves for EMCA and CISS MR, respectively. The violation of Onsager's relation is characterized by the change of zero-bias conductance upon switching the electrode magnetization. **d** In a CISS device, the ferromagnet-molecule interface exhibits magnetization (M), spin-orbit coupling (SOC), chirality (χ), and dissipation. A chiral chain model (light blue) is adopted to represent the interface with coexisting M, SOC, χ, and dissipation. (**e**) At the interface, the wave function is exponentially localized to one side due to the non-Hermitian skin effect (NHSE) when the current flows. Merely NHSE leads to EMCA - another interpretation of EMCA besides the spin polarization. If an impurity state(circle) exists on the molecule side, the asymmetric wave function due to NHSE can control this state occupied (electron-trapping) or empty. **f** Schematics of energy profile for the electron-trapping state and no trap state as two metastable phases. NHSE drives the switch between two phases by reserving M (or χ), *i.e.* the magnetochiral charge pumping.

polarization. The CISS MR increases with bias and molecule length and can be even larger than 60% in reports[18–20], although the FM electrode, such as Ni, exhibits only 20% spin polarization. Despite the tremendous theoretical efforts[5] that were made to interpret the induced spin polarization by chiral molecules, it is still impossible to rationalize the giant CISS MR ratio by assuming even 100% spin polarization in the molecule and matching it to the FM contact (20%).

Furthermore, the CISS MR exhibits fundamentally distinct symmetry[8,21–25] in the current-voltage (I–V) behavior (see Table 1 and Fig. 1b, c) from another known chirality-induced phenomenon called electrical magnetochiral anisotropy (EMCA)[26]. EMCA refers to the resistance that depends on the current (**I**) and magnetic field (**B**) for a chiral conductor, $R^{\chi} = R_0(1 + \alpha B^2 + \beta^{\chi}\mathbf{B}\cdot\mathbf{I})$, where $\beta^{\chi} = -\beta^{-\chi}$ and $\chi = \pm$ stands for chirality. The B^2 term represents the ordinary MR while the $\mathbf{B}\cdot\mathbf{I}$ term represents the unidirectional resistance like a diode (see Fig. 1b). EMCA was observed in many chiral solids[26–32], where the MR is usually a few percent or even less. In addition, the intrinsic magnetic order plays a similar role to the magnetic field and enhances EMCA in experiments[29]. As summarized in Table 1, EMCA respects Onsager's reciprocal relation while CISS MR violates such reciprocity. Figure 1c illustrates the I–V relation of CISS MR. Onsager's reciprocal theorem originates in the microscopic reversibility of thermodynamic equilibrium and poses strict constraints on macroscopic conductivity[33]. The reciprocity requires that two-terminal conductance remains unchanged as reversing time $(B/M \to -B/-M)$, i.e., $G(B/M) = G(-B/-M)|_{V\to 0}$[33–35], which holds for EMCA and ordinary transport but not for CISS MR. Actually, EMCA can be derived by weakly perturbing the equilibrium ground state to the nonlinear order in the semiclassical theory[36–38] while CISS MR will require understanding the far out-of-equilibrium phase. We stress that device ground states for $\pm M$ at thermodynamic equilibrium should be rigidly equivalent because they are time-reversal partners to each other, and the equilibrium phase is unchanged in time by definition. Then, it is puzzling to observe varied zero-bias conductance between $\pm M$ in a CISS device.

The chiral molecule was commonly regarded as a spin filter[3,4] in which electrons exhibit opposite spin polarization after transmitting through the chiral molecule from opposite directions. However, recent theoretical works[21,22,39] pointed out that reflected electrons by the chiral molecule exhibit the same spin polarization as transmitted ones, and the chiral molecule actually acts as a spin polarizer[39]. As illustrated in Fig. 1a, the right (left) moving electrons can be polarized to spin right (left) for both transmitted and reflected electrons. Such a direction-dependent spin polarization was also revealed by recent ab initio calculations[40]. The right(left)-moving electrons generate low (high) resistance if their spin is parallel (anti-parallel) to the polarization of the FM electrode. Therefore, the I–V curve exhibits a diode-like feature (see Fig. 1b), i.e., current-direction-dependent conductance. The sign of reification switches if reversing the magnetization or molecule chirality, presenting EMCA. The spin polarization in the context of CISS directly leads to the EMCA transport, consistent with recent experiments with chiral conductors[26–32]. To understand the CISS MR from chiral molecules, however, we need a mechanism beyond the spin polarization because of the fundamental symmetry reason, regardless of the origin of spin-orbit coupling (SOC) from metal contacts or organic molecule[7,8,17].

In the zero bias limit, many CISS experiments[12,14,17,23] showed a clear violation of Onsager's relation by $G(M) \neq G(-M)|_{V\to 0}$, indicating

Table 1 | Summary of CISS MR and EMCA in experiments

MR-type	Materials	Resistance	Onsager's Relation
CISS-MR	Insulating chiral molecules	1 ~ 1000MΩ $MR \geq 60\%$	Violated $G(M) \neq G(-M)\vert_{V\to 0}$
EMCA	Chiral metals/ semiconductors	1 ~ 100Ω MR ~ 1% or smaller	Preserved $G(M) = G(-M)\vert_{V\to 0}$

The conductance is represented by $G(V, M)$, which depends on the bias voltage (V) and electrode magnetization (M). Representative values of resistance and magnetoresistance (MR) are taken from refs. 12,14–16,18,23 for CISS-MR and refs. 26–32 for EMCA.

that switching M drives the system to different metastable states and consequently leads to varied conductance. If so, what kind of metastable states matter here? Given that a CISS device and EMCA share the same symmetry condition, both inversion symmetry-breaking and time-reversal symmetry-breaking, what causes different transport behaviors between CISS and EMCA? Answers to these questions will help to understand the nature of CISS. In experiments, EMCA involves metals or doped semiconductors, while CISS MR commonly measures insulating chiral molecules (see Table 1). In CISS, for example, the typical resistance is in the GΩ scale[11]. Therefore, we speculate that the insulating nature of chiral molecules can be essential for understanding CISS MR, which was rarely appreciated in the literature. In a molecular tunneling junction, it is natural to use the potential barrier (U) to characterize the tunneling conductance. Then we aim to resolve how electrode magnetization ($\pm M$) or chirality modifies the potential barrier when charge flows through the CISS device. Some recent works[9,10,25,41] discussed that induced spin accumulation might change the effective potential at non-equilibrium. But this spin accumulation scenario would apply to chiral conductors and thus, fail to distinguish chiral insulators from chiral metals. In this work, we explore the induced charge trapping that directly modulates the potential, which is significant for the insulating chiral molecule but negligible for the chiral metals/doped-semiconductors. It should be noted that carrier trapping is a commonly observed phenomenon in molecular transport[42–45] and usually exhibits a long-lived lifetime[46–49].

In this article, we propose that the CISS MR originates in charge-trapping-induced tunneling-barrier modification (as illustrated in Fig. 1e). At the FM-molecule interface (Fig. 1d) with coexisting magnetism, chirality, and SOC, a non-Hermitian skin effect (NHSE)[50–55] appears, which is widely demonstrated in topological systems like photonic lattices and quantum devices[56–60]. NHSE generates extensive exponentially localized eigenstates at two sides of the interface due to dissipation as current flows (see Fig. 1e). The localization direction, which reverses as flipping magnetism or chirality, leads to occupied or empty impurity/defect levels in the molecule side of the interface, and thus generates electron/hole-trapping, which we call the magnetochiral charge pumping effect. The trapped charge has a long lifetime as a metastable state (Fig. 1f), survives at zero bias, and consequently alters the electron tunneling barrier in the whole device. Therefore, CISS MR refrains from Onsager's relation due to charge trapping and can show significantly larger MR than expected from the electrode spin polarization. The charge-trapping model is consistent with the experimental observation that local charging at the FM-molecule interface lasts long and modifies the surface potential[61,62]. We further anticipate that CISS MR may appear without FM electrodes but with an external magnetic field because NHSE also exists in this case, as verified by very recent experiments[63,64]. Because charge trapping requires stabilization by the insulating layer, we predict that CISS MR will diminish and evolve into EMCA if the chiral insulator becomes more metallic. The magnetochiral charge pumping will provide further insights into the magnetism-modulated charge transfer in chirality-related chemical and biological reactions[65–69].

Results

The induced spin polarization in chiral molecules was frequently regarded as the MR ratio in literature. However, resistance rather than spin is the directly measured quantity in transport. Thus, we circumvent the illusive spin polarization[70] and focus on MR in this work. As discussed above, the nonequilibrium spin polarization in the context of CISS directly leads to EMCA, which is independent of model details such as the origin of SOC. In the following, we will reveal NHSE at the FM-molecule interface. Because NHSE can alter the occupation of defect/disorder states in the molecule side and then lead to charge trapping there. The trapped charge can survive even at zero bias and modulate the tunneling barrier sensitively, circumventing Onsager's reciprocal relation. Finally, we will propose a simple tunneling barrier model that can reproduce essential features of CISS MR and extract the barrier information from experiments.

Non-Hermitian skin effect

EMCA can also be understood by NHSE besides the spin polarization scenario. NHSE is widely studied in dissipative (nonequilibrium) systems such as photonic lattices and is characterized by exponentially localized eigen wavefunctions at system boundaries, as a topological phenomenon. In realistic materials, NHSE requires dissipation and breaking of both time-reversal symmetry and inversion symmetry[53,56,71]. In the CISS device (Figs. 1d, 2a), the FM-molecule interface is the only region combining three ingredients, M (time-reversal breaking), χ (inversion-breaking), and SOC (coupling M and χ together), satisfying the NHSE condition. In the following, we employ a chiral chain model consisting of two parts, as illustrated in Fig. 2a. The left part represents the interface region, which includes both M and SOC. The right part models the insulating molecule region. In addition, we introduce an impurity site between these two parts to serve as a charge-trapping center. Neither the molecule region nor the impurity site includes M or SOC to represent a realistic molecular device.

We construct a tight-binding model for the chiral chain, incorporating orbital-dependent dissipation in the left part (see Supplementary Information for details). This left part exhibits NHSE, characterized by localized eigenstates at the boundaries. As illustrated in Fig. 2c, d, positive magnetization ($+M$, $\Rightarrow$) causes wave functions to localize at the left open boundary, while negative magnetization ($-M$, $\Leftarrow$) generates states localized in the junction region. The impurity state, due to its coupling with the interface part, is highly sensitive to NHSE. Depending on the magnetization ($\pm M$), its wave function is either drawn away from or more localized at the impurity site (see more details in Supplementary Information). In contrast, wave functions in the molecule part are only marginally affected by NHSE. NHSE induces unidirectional tunneling through the system. For instance, the left-side localization of eigenstates (Fig. 2d) enhances electron tunneling from right to left while suppressing tunneling in the opposite direction, as reported in the literature[53]. Consequently, the unidirectional tunneling resistance can be reversed by altering either M or χ, giving rise to EMCA, which respects the general reciprocity (also see Supplementary Fig. S7). Thus, EMCA serves as the transport signature of NHSE, while NHSE represents the spectroscopic manifestation of the system out of equilibrium. Here, solely NSHE cannot violate the Onsager's relation to produce CISS-type MR.

We note that NHSE comes from the interplay between M, χ, SOC, and dissipation. It vanishes if one of them disappears in our model. Specially, dissipation is essential for NHSE. In a CISS device, it

https://doi.org/10.1038/s41467-024-55433-1

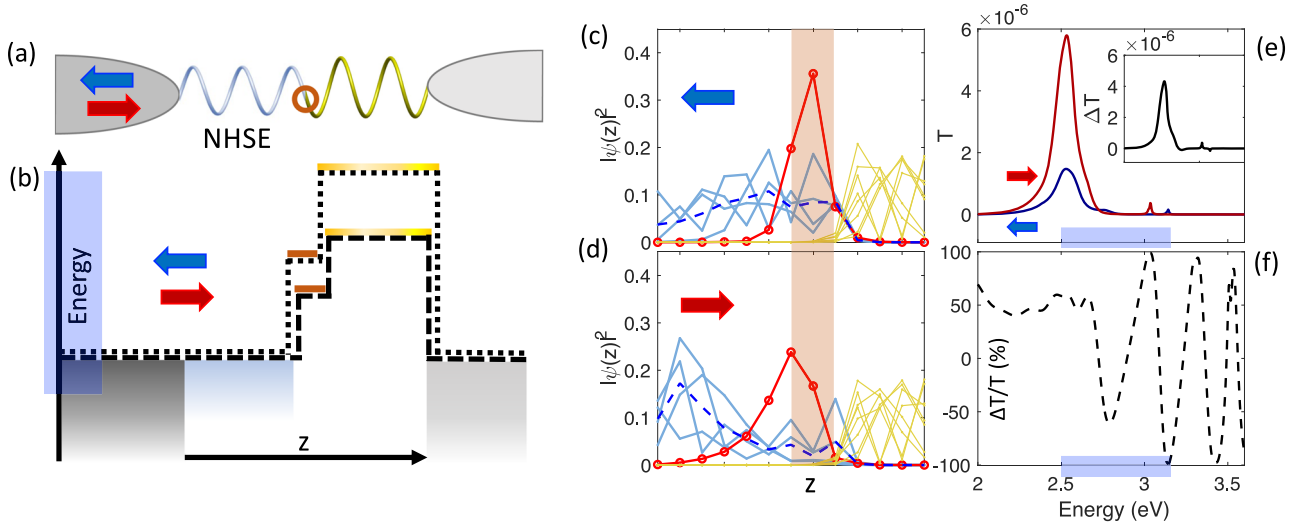

Fig. 2 | Barrier modification in a molecular device. a The two-terminal device includes an interface region (with M, SOC, and χ) with non-Hermitian skin effect (NHSE) and an ordinary molecule region (with only χ). **b** Illustration of the potential profile across the device. The charge trapping sensitively modifies the energy of the impurity state (dark orange) and the molecule state (yellow) but leaves the interface region nearly unchanged because the interface is much more metallic than the molecule region. **c**, **d** show the wavefunction distribution of interface (light blue), impurity (red), and molecule (yellow) states due to NHSE at opposite M. The blue dashed curve represents the average of interface wave functions. These states are located in an energy window indicated by the blue shadow along the energy axis in (**b**, **e**, **f**). The impurity occupation probability is evaluated in the red shadow region that is centered at the impurity site. (e) The transmission probability (T) at different chemical potentials for opposite M is calculated for the two-terminal device shown in (**a**). **f** shows the corresponding ratio of transmission change.

originates from the current-related dissipation due to scattering by lattice, disorder, interface, etc. Because the chiral molecule is typically anisotropic, conduction channels with distinct orbital features (e.g., π and σ orbitals) may dissipate differently. Thus, we include orbital-dependent dissipation in the model. In addition, the role of dissipation/dephasing was discussed to study spin polarization in earlier theoretical works on CISS[72–74]. We should also note that NHSE cannot emerge from the finite-temperature effect at thermodynamic equilibrium, because energy dissipation and gain between electrons and environment (e.g., lattice vibrations[9]) compensate each other in this case.

Charge trapping and barrier modification

When dissipation diminishes at zero bias, NHSE disappears. Then, merely NHSE cannot explain the violation of Onsager's reciprocity. Therefore, we need the charge trapping effect which survives at zero bias.

Conceive a localized impurity level between left and right parts in the model of Fig. 2a, which may come from interface states (e.g., thiol bonds[75,76]), structural defects, or extrinsic impurities (e.g., oxygen[77] or water[78,79]). This state acts as charge(electron/hole)-trapping centers in the insulating molecule side. The key question is how the charge-trapping can be controlled by M and χ, to which we attribute NHSE.

As shown above, the impurity state wavefunction is also modified by NHSE. To avoid confusion, we initialize zero spin polarization for the impurity in our model. For simplicity, we assume that one impurity traps only an electron (the unipolar transport case), which can be easily generalized to hole trapping or bipolar transport. For $-M$ in Fig. 2c, NHSE tends to keep the impurity state occupied by an electron. Even if it is empty, NHSE enhances electron transfer from left to right to fill the impurity level. In contrast, NHSE keeps the impurity level empty at $+M$. We should stress that the occupied and unoccupied states are metastable on the energy surface (see Fig. 1f) and remain robust at zero bias. Here, NHSE plays a driving force to swap the impurity level between occupied and empty phases, which depends on $\pm M$ (also χ). The charge trapping can sensitively tune the tunneling barrier in a CISS device, leading to magnetization-(also chirality-) dependent resistance even at zero bias.

To quantitatively demonstrate the barrier modification, we calculated the zero-bias conductance for the device shown in Fig. 2a. For a given magnetization M, we evaluated the charge-trapping probability (ρ_M) from the wave function localization at the impurity site (integrated in the red shadow region in Fig. 2c, d, where $\rho_{+M/-M} \approx 0.85/0.45$). When an electron is trapped, it can elevate the electrostatic potential by V_0 in the impurity and molecule regions while leaving the interface region largely unchanged, due to the insulating nature of the former and the metallic character of the latter. We estimated $V_0 = \frac{e^2}{4\pi\epsilon d} \approx 0.4$ eV, considering a 3 ~ 5 nm characteristic thickness of the chiral molecule layer and $\epsilon = 2.1\epsilon_0$[80]. For simplicity, we applied a rigid onsite potential shift of $V_0\rho_M$ to impurity and molecule parts. We then calculated the two-terminal tunneling probability for $\pm M$ ($T_{\pm M}$) after attaching a ferromagnetic electrode and an ordinary lead. To demonstrate the violation of Onsager's relation, we focus on the zero-bias conductance at a given chemical potential (see Fig. 2e), in which the dissipation vanishes but charge trapping remains. The resulting $T \ll 1$ because it originates from potential barrier tunneling through the insulating molecule. The electron barrier height equates to the energy difference between the electrode's chemical potential and the molecule's lowest unoccupied molecular orbital(see Fig. 2b). Consequently, even a small barrier modification due to different ρ_M values can lead to a large change in T ($\Delta T = T_{-M} - T_{+M}$), characterizing the violation of Onsager's relation. Figure 2f shows that the ratio of T change [$(\Delta T/(T_{-M} + T_{+M}))$] can exceed 50% and even approach 100% for certain chemical potentials. This further indicates that both the sign and magnitude of CISS MR depend not only on χ and M but also on device-specific details such as the chemical potential. In addition, we note that more complex potential profiles also yield a large T change ratio (see Supplementary Information) because T is quite sensitive to potential changes in the tunneling regime.

We stress that the spin polarization may be relevant to CISS MR but cannot explain the reciprocity violation. The trapped charge by the insulating molecule is a key ingredient to breaking the microscopic reversibility and circumventing the Onsager relation. This also explains why conducting chiral crystals, in which charge cannot be trapped or trapped charge has marginal influence in resistance, exhibit EMCA rather than CISS MR. Our model also rationalizes why the CISS MR can

significantly exceed the spin polarization ratio in the FM electrode. This is because the modified barrier dramatically amplifies the tunneling conductance, as demonstrated by our calculations. In addition, the FM-molecule interface model naturally breaks the 180° rotation symmetry of the device, coinciding with a recent discussion on the symmetry requirement of CISS MR[81].

An effective barrier model

The trapped charge (electron or hole) can modify the injection barrier at the metal-molecule interface and/or change the barrier profile (e.g., shape, height, width) in a complicated way. For further simplicity, we present an effective model by considering a rectangular barrier with height U_0 and a barrier modulation δU, in the spirit of the widely adopted Simmons model to simulate the electron transport in molecular junctions[82]. If the molecule conducts electrons, electron or hole trapping indicates an increase or decrease in the barrier, respectively, and vice versa for the hole-conducting case.

We can estimate the transport through a rectangular barrier $U = U_0 + \delta U$ in the case of $eV < U$,

$$I = g[(U + eV/2)e^{-A*\sqrt{U+eV/2}} - (U - eV/2)e^{-A*\sqrt{U-eV/2}}], \quad (1)$$

where $A = \frac{4\pi l\sqrt{2m^*}}{h}$, l is the barrier width, g is a constant in unit of conductance, m^* is the effective mass. Here, we symmetrize Eq. (1) for $\pm V$ compared to the Simmons model[82].

As shown in Fig. 3, I–V curves calculated by Eq. (1) well reproduce the symmetry of CISS-MR and the variation of zero-bias conductance. We take $U_0 = 5eV$, $\delta U = 0.2\,eV$, and $m^* = 0.28\,m_e$[80], where m_e is the free electron mass. The MR ratio enlarges slightly as increasing bias but increases dramatically as increasing the barrier width. In literature[83], the CISS-driven spin polarization (P) is frequently defined via the current change for $\pm M$,

$$P = \frac{|I(+M) - I(-M)|}{I(+M) + I(-M)}, \quad (2)$$

which leads to an unphysical abrupt drop of P near the zero bias. Instead, we define a similar quantity termed normalized MR ($\widetilde{MR}$) by the change of conductance $G = dI/dV$ (or resistance) as,

$$\widetilde{MR} = \frac{|G(+M) - G(-M)|}{G(+M) + G(-M)} \equiv \frac{|R(-M) - R(+M)|}{R(-M) + R(+M)}, \quad (3)$$

which exhibits a more reasonable bias dependence near the zero bias region. Consistent with experimental observations[18–20], we find that $\widetilde{MR}$ increases as increasing the barrier width because barrier width is proportional to A in Eq. (1). As shown in Fig. 3, one can reach a high $\widetilde{MR}$ up to 100% by engineering device parameters such as the barrier width.

We stress that $\widetilde{MR}$ qualitatively differs from the so-called spin polarization (P_χ) in CISS literature despite that they are frequently considered to be equivalent to each. If we follow the tunneling magnetoresistance picture[84] regarding tunneling between the FM electrode with spin polarization P_{FM} and chiral molecule, we get $\widetilde{MR} = P_\chi P_{FM} \neq P_\chi$ except $P_{FM} = 100\%$ which is unrealistic. Known the low P_{FM} in ordinary FM, $\widetilde{MR} \leq P_{FM}$ obviously contradicts the high $\widetilde{MR}$ in experiments. Thus, we suggest that $\widetilde{MR}$ may serve a more proper terminology to characterize CISS transport compared to the so-called spin polarization. In our theory, the large $\widetilde{MR}$ value is caused by the nonlinear amplification of the barrier tunneling, which is indirectly related to spin polarization.

Discussions and outlook

The charge trapping due to NHSE circumvents Onsager's relation and reproduces the major symmetry of CISS transport. The charge trapping may occur at the molecule-metal interface, defects, disorders, or impurities, and its microscopic origin may vary among different molecules and devices. Nevertheless, we can make insightful predictions from the proposed mechanism that relies on NHSE and charge trapping.

(i) If a device traps both electrons and holes, one can expect the ideal barrier modification as $U = U_0 \pm \delta U$ for $\pm M$. (ii) If a device traps only electrons/holes, the barrier is switched between U_0 and $U = U_0 \pm \delta U$. Here, a salient feature is that the conductance for one of $\pm M$ is comparable to the $M = 0$ case, showing asymmetric MR between $\pm M$. (iii) If the device does not efficiently trap charge, the CISS MR may diminish and change to EMCA. This is consistent with the EMCA observed in metallic or nearly metallic chiral solids[26–31] where charge trapping can be screened by the metallic background. EMCA may also occur for an insulating chiral molecule if the device is ideally clean without a charge-trapping center. (iv) Because NHSE and EMCA do not necessarily require an FM electrode, we anticipate that CISS MR may also occur with ordinary electrodes in an external magnetic field if the charge trapping condition is satisfied. For example, electrons in a metallic chiral crystal can feel the magnetic field by the Lorentz force, and charge trapping may occur at the crystal interface with another insulating layer that is essential to determine the sign of MR. In this case, SOC in materials/electrodes is not essential for CISS MR because the magnetic field directly couples to the electron motion (orbital). (v) The amplitude of EMCA (also NHSE) is scaled by SOC in electrodes[7,8] because organic molecules usually have negligible SOC. So CISS MR is also scaled by electrode SOC. The electrode dependence was confirmed by observing significantly different MR with Au and Al electrodes in ref. 17 recently. We should stress that CISS-type MR is directly determined by the charge-trapping effect despite that it is related to the SOC. In some cases, it is possible to observe that CISS MR is less sensitive to SOC while coexisting EMCA is more sensitive to SOC. For example, when SOC is strong enough to enforce a charge trapping probability of nearly 100%, further increasing SOC will hardly change CISS MR despite enhancing EMCA. (vi) The charge trapping usually comes with local structural distortion at the interface or inside the molecule. Such distortion may be detected via the change of atomic bonding, for example, by the Raman spectrum.

Furthermore, we can include the I-V asymmetry due to EMCA or device asymmetry with (1) and provide a general formula to describe the I–V relation for chiral molecular devices,

$$I = g[(U + eV/2)e^{-A*\sqrt{U+eV/2}} - (U - eV/2)e^{-A*\sqrt{U-eV/2}}](1 - \gamma V), \quad (4)$$

where $\gamma = (\gamma_0 + \gamma_M^\chi)/R_0$ includes γ_M^χ due to EMCA and γ_0 is a constant caused by device asymmetry such as different electrodes or molecular dipole. Equation (4) indicates a crossover from CISS MR to EMCA if γ_M^χ is dominant or potential change (δU) is negligible, as discussed above.

We suggest that one can extract key parameters, including γ and U, by fitting experiments with Eq. (4). For example, we successfully fit the original experimental I-V relation using Eq. (4) in Fig. 4. For the same device with a given chirality, we globally fit two sets of I–V curves with $\pm M$ by using the same g and A because they are invariant for $\pm M$.(see more details in Supplementary Information) We obtain the barrier change $\delta U = 0.3$, 0.1 and 0.5 eV for experiments by Abendroth et al.[61], Gosh et al.[62] and Al-Bustami et al.[18]. The large δU (also large $\delta U/U$) well rationalizes that Al-Bustami et al. observed a much larger $\widetilde{MR}$ than the other two works. Even if we know little atomic configuration of the device, we can still use the barrier model to rationalize CISS experiments.

Furthermore, Abendroth et al. [61] and Gosh et al. [62] also observed the work function change ~ 0.1 eV due to switching magnetization for chiral films on the FM substrate and discussed its correlation to CISS. As shown above, we obtain a similar magnitude in the charge tunneling barrier change (δU) by fitting their transport results. The barrier is

https://doi.org/10.1038/s41467-024-55433-1

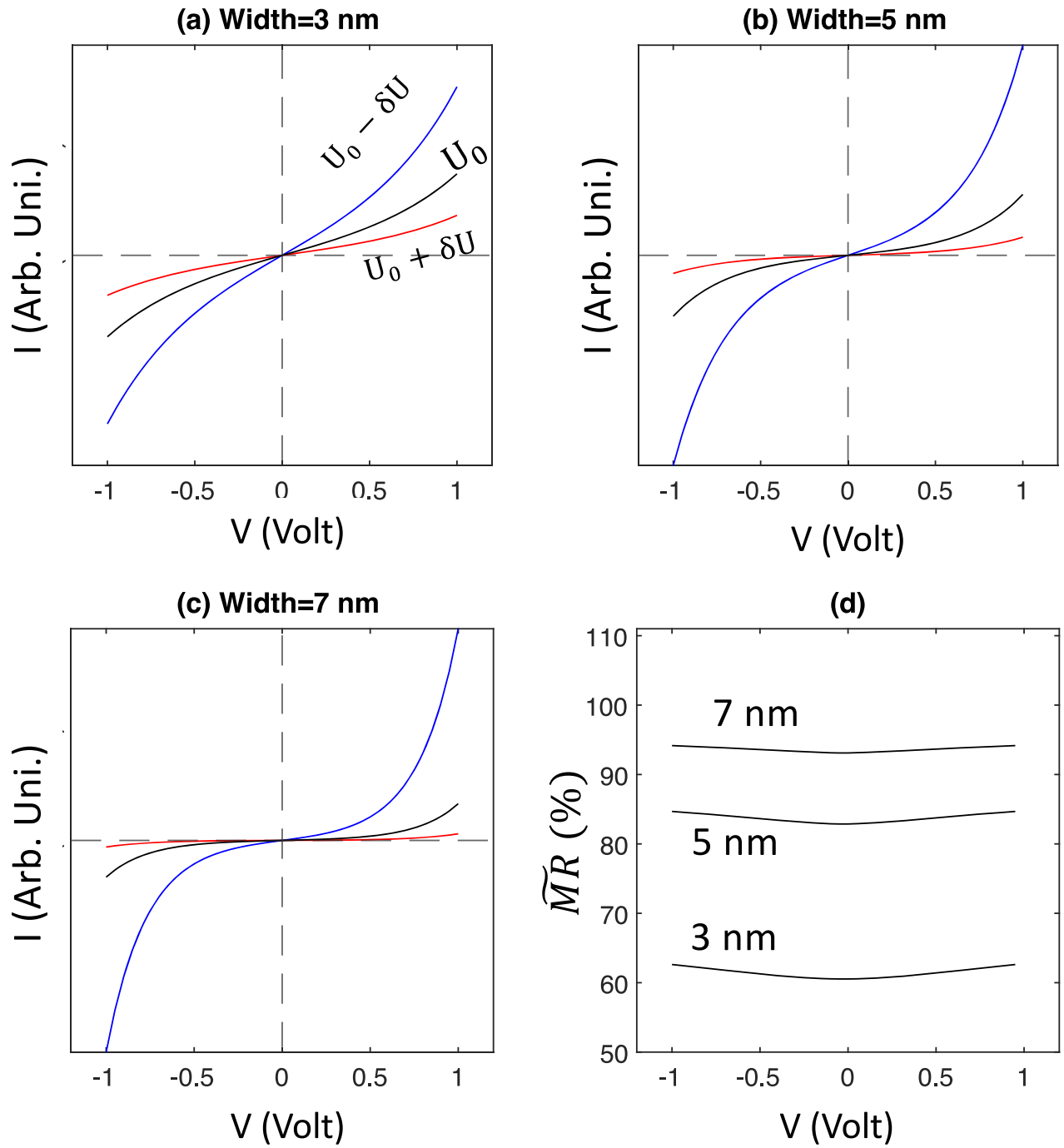

Fig. 3 | The I-V curves calculated from Eq. a–c The MR increases dramatically as the width increases. **d** The normalized MR [$\widetilde{MR}$, defined in Eq. (3)] increases with the width.

related to the energy offset between the metal Fermi surface and molecule levels, and the work function is related to the difference between the metal Fermi surface and vacuum. Because both can be modified by the surface/interface charging effect, it is not surprising to expect changes of comparable magnitude due to magnetization flipping. In addition, Abendroth et al. showed negligible surface potential change after they neutralized the surface charging, indicating a direct correlation between the charging and CISS[61]. This further supports that the trapped-charge-induced barrier modulation can be a key ingredient to understanding CISS transport, which correlates to the work function change.

The magnetochiral charge pumping is a dynamic process characterized by complex interfacial interactions. When current flows through a chiral molecular device, magnetization/magnetic field switching first reverses the interface wavefunction localization direction via NHSE. This process requires a finite time to modify the charge trapping state, which is typically close to or larger than the structural relaxation time due to associated lattice distortions. The barrier change (0.1 ~ 1 eV) cannot be compensated by the Zeeman energy from electrode magnetization flipping (around 1 meV). In this open system, the required energy to alter the potential profile is provided by the external current flow. Future work should focus on establishing a quantitative description of the dynamic interplay between NHSE and charge trapping to elucidate the underlying microscopic mechanisms.

Our work reveals a fundamental mechanism of how magnetism or magnetic field modifies the charge distribution at the metal-organic

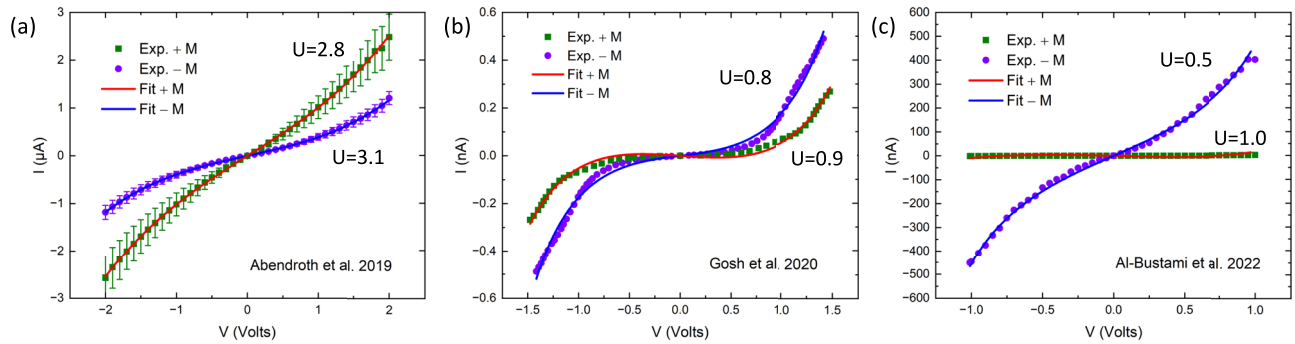

Fig. 4 | Fitting the experimental results with the barrier model. The experimental data were obtained from (**a**) ref. 61, (**b**) ref. 62 and (**c**) ref. 18. The extracted barrier height (U) is marked with a corresponding I–V curve.

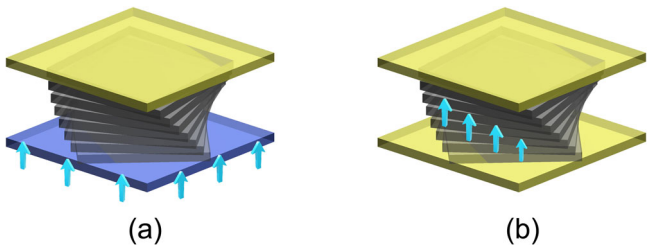

Fig. 5 | CISS platforms by twisted van der Waals layers sandwiched between vertical electrodes. The electrodes can be either metals or metallic/semimetallic van der Waals materials. Blue arrows indicate the magnetic material or a magnetic field. Magnetism can appear in one/both electrodes (**a**) and/or (**b**) in the twisted material. If the twisted layers are insulating, CISS-type MR can occur. If it is more conducting, it may exhibit EMCA. The role of SOC can be examined in different electrodes like graphite and transition metal dichalcogenides.

interface through nonequilibrium dynamics. Besides chiral molecular transport, our work can also explain the magnetic substrate-modulated charge reorganization in protein-protein association[65,66], in which the magnetochiral charge pumping changes the electrostatic potential of proteins by switching the substrate magnetization. It paves a pathway to modulate chemistry and biology processes, which commonly involve chiral materials, by controlling the charge transfer or the long-range electrostatic potential.

We have another outlook that the recently discovered twisted van der Waals materials[85–87] provide versatile platform for the CISS effect. In twisted bilayer graphene and twisted transition-metal dichalcogenides[88–91], the in-plane transport has been extensively studied for flat-band-driven phenomena such as unconventional superconductivity, Mott insulating states, and Chern insulators. We conceive a two-terminal vertical device where two electrodes sandwich twisted bilayers or multiple layers, as illustrated in Fig. 5. It was recently proposed that flat bands significantly enhance the EMCA effect in twisted bilayer graphene[37]. The EMCA comes from the coexistence of magnetization (or magnetic field) and chirality. Since twisted layers are chiral, we introduce magnetism to either one electrode and/or twisted layers. Many van der Waals materials are magnetic, such as insulating CrI_3[92], semiconducting $MnBi_2Te_4$[93], and metallic Fe_3GeTe_2[94] and Cr_3Te_4[16]. In addition, twisting between van der Waals electrodes can also play the role of chirality. The vertical resistance[95] can be measured for the opposite magnetization and for opposite twist angles. If chiral layers are insulating, we anticipate CISS-like MR. If they are metallic, we expect EMCA-like MR. In most of the present CISS devices, a thin layer of gold is technically required to protect the ferromagnetic film. This gold layer results in difficulties in examining the influence of substrate SOC[7,8]. In Fig. 5, electrodes can also be made of van der Waals materials (such as graphite) with negligible SOC, which circumvents this problem as well as the complexity of metal-organic molecule junction. Therefore, van der Waals materials provide a versatile platform to investigate the relation of CISS with SOC, magnetism, and chiral layer insulation. It would be more exciting to examine the influence of flat bands[37,85], correlation effects, and even superconductivity in CISS[96].

Note: During the review of the manuscript, our predictions (ii) &(iv) on the asymmetric magnetoresistance in an external magnetic field were realized in chiral gold nanocrystals[63], in which metallic gold core shows the chiral morphology and insulating surface capping layer traps the charge in the magnetochiral charge pumping. A similar asymmetric magnetoresistance was also observed in a chiral supermolecular crystal with solely a magnetic field where the charge trapping effect was observed[64]. Our prediction (v) on the coexistence of EMCA and CISS was reported in chiral single-molecule junction measurements[97] very recently, in which EMCA is sensitive to SOC while CISS is nearly independent of SOC, and the reciprocal relation is violated at zero bias.

Data availability

The data for the charge barrier model in a chiral molecular and the transmission probability for the two-terminal device is available in Zenodo at https://doi.org/10.5281/zenodo.14205821. Supplementary information that supports this work is available upon request to the corresponding author.

Code availability

The Mathematica code used to calculate the charge barrier model, modify the impurity potential under reversed magnetism, and calculate the transmission probability using the non-equilibrium Green's function formalism is available in Zenodo at https://doi.org/10.5281/zenodo.14205821.

References

1. Kelvin, W. T. B. *The Molecular Tactics of a Crystal* (Clarendon Press, 1894).
2. Gohler, B. et al. Spin selectivity in electron transmission through self-assembled monolayers of double-stranded DNA. *Science* **331**, 894 – 897 (2011).
3. Naaman, R. & Waldeck, D. H. Chiral-induced spin selectivity effect. *J. Phys. Chem. Lett.* **3**, 2178–2187 (2012).
4. Naaman, R., Paltiel, Y. & Waldeck, D. H. Chiral molecules and the electron spin. *Nat. Rev. Chem.* **3**, 250–260 (2019).
5. Evers, F. et al. Theory of chirality induced spin selectivity: Progress and challenges. *Adv. Mater.* **34**, 2106629 (2022).
6. Yan, B. Structural chirality and electronic chirality in quantum materials. *Annu. Rev. Mater. Res.* **54**, 97–115 (2024).

7. Gersten, J., Kaasbjerg, K. & Nitzan, A. Induced spin filtering in electron transmission through chiral molecular layers adsorbed on metals with strong spin-orbit coupling. *J. Chem. Phys.* **139**, 114111 (2013).
8. Liu, Y., Xiao, J., Koo, J. & Yan, B. Chirality-driven topological electronic structure of dna-like materials. *Nat. Mater.* **6**, 638–644 (2021).
9. Das, T. K., Tassinari, F., Naaman, R. & Fransson, J. Temperature-dependent chiral-induced spin selectivity effect: Experiments and theory. *J. Phys. Chem. C* **126**, 3257–3264 (2022).
10. Hedegård, P. Spin dynamics and chirality induced spin selectivity. *J. Chem. Phys.* **159**, https://doi.org/10.1063/5.0160233 (2023).
11. Xie, Z. et al. Spin specific electron conduction through DNA oligomers. *Nano Lett.* **11**, 4652–5 (2011).
12. Kiran, V. et al. Helicenes-A New Class of Organic Spin Filter. *Adv. Mater.* **28**, 1957–1962 (2016).
13. Varade, V. et al. Bacteriorhodopsin based non-magnetic spin filters for biomolecular spintronics. *Phys. Chem. Chem. Phys.* **20**, 1091–1097 (2018).
14. Liu, T. et al. Linear and nonlinear two-terminal spin-valve effect from chirality-induced spin selectivity. *ACS Nano* **14**, 15983–15991 (2020).
15. Kim, Y.-H. et al. Chiral-induced spin selectivity enables a room-temperature spin light-emitting diode. *Science* **371**, 1129–1133 (2021).
16. Qian, Q. et al. Chiral molecular intercalation superlattices. *Nature* **606**, 902–908 (2022).
17. Adhikari, Y. et al. Interplay of structural chirality, electron spin and topological orbital in chiral molecular spin valves. *Nat. Commun.* **14**, 5163 (2023).
18. Al-Bustami, H. et al. Atomic and molecular layer deposition of chiral thin films showing up to 99% spin selective transport. *Nano Lett.* **22**, 5022–5028 (2022).
19. Kulkarni, C. et al. Highly efficient and tunable filtering of electrons' spin by supramolecular chirality of nanofiber-based materials. *Adv. Mater.* **32**, 1904965 (2020).
20. Mishra, S. et al. Length-dependent electron spin polarization in oligopeptides and DNA. *J. Phys. Chem. C* **124**, 10776–10782 (2020).
21. Yang, X., Wal, C. H. V. D. & Wees, B. JV Spin-dependent electron transmission model for chiral molecules in mesoscopic devices. *Phys. Rev. B* **99**, 024418 (2019).
22. Yang, X., van der Wal, C. H. & van Wees, B. J. Detecting chirality in two-terminal electronic nanodevices. *Nano Lett.* **20**, 6148–6154 (2020).
23. Naaman, R. & Waldeck, D. H. Comment on "Spin-dependent electron transmission model for chiral molecules in mesoscopic devices". *Phys. Rev. B* **101**, 026403 (2020).
24. Yang, X., van der Wal, C. H. & van Wees, B. J. Reply to "comment on 'spin-dependent electron transmission model for chiral molecules in mesoscopic devices"'. *Phys. Rev. B* **101**, 026404 (2020).
25. Dalum, S. & Hedegard, P. Theory of chiral induced spin selectivity. *Nano Lett.* **19**, 5253–5259 (2019).
26. Rikken, G. L. J. A., Fälling, J. & Wyder, P. Electrical magnetochiral anisotropy. *Phys. Rev. Lett.* **87**, 236602 (2001).
27. Rikken, G. L. J. A. & Avarvari, N. Strong electrical magnetochiral anisotropy in tellurium. *Phys. Rev. B* **99**, 245153 (2019).
28. Pop, F., Auban-Senzier, P., Canadell, E., Rikken, G. L. & Avarvari, N. Electrical magnetochiral anisotropy in a bulk chiral molecular conductor. *Nat. Commun.* **5**, 3757 (2014).
29. Aoki, R., Kousaka, Y. & Togawa, Y. Anomalous nonreciprocal electrical transport on chiral magnetic order. *Phys. Rev. Lett.* **122**, 057206 (2019).
30. Inui, A. et al. Chirality-induced spin-polarized state of a chiral crystal $CrNb_3S_6$. *Phys. Rev. Lett.* **124**, 166602 (2020).
31. Shiota, K. et al. Chirality-induced spin polarization over macroscopic distances in chiral disilicide crystals. *Phys. Rev. Lett.* **127**, 126602 (2021).
32. Niu, C. et al. Tunable nonreciprocal electrical transport in 2D Tellurium with different chirality. *Nano Lett.* **23**, 8445–8453 (2023).
33. Onsager, L. Reciprocal relations in irreversible processes. ii. *Phys. Rev.* **38**, 2265–2279 (1931).
34. Landau, L. & Lifshitz, E. in *Statistical Physics*.(Butterworth-Heinemann, Oxford, 1980).
35. Büttiker, M. Symmetry of electrical conduction. *IBM J. Res. Dev.* **32**, 317–334 (1988).
36. Ideue, T. et al. Bulk rectification effect in a polar semiconductor. *Nat. Phys.* **13**, 578–583 (2017).
37. Liu, Y., Holder, T. & Yan, B. Chirality-induced giant unidirectional magnetoresistance in twisted bilayer graphene. *Innovation* **2**, 100085 (2021).
38. Kaplan, D., Holder, T. & Yan, B. Unification of nonlinear anomalous hall effect and nonreciprocal magnetoresistance in metals by the quantum geometry. *Phys. Rev. Lett.* **132**, 026301 (2024).
39. Wolf, Y., Liu, Y., Xiao, J., Park, N. & Yan, B. Unusual spin polarization in the chirality-induced spin selectivity. *ACS Nano* **16**, 18601–18607 (2022).
40. Naskar, S., Mujica, V. & Herrmann, C. Chiral-induced spin selectivity and non-equilibrium spin accumulation in molecules and interfaces: A first-principles study. *J. Phys. Chem. Lett.* **14**, 694–701 (2023).
41. Alwan, S. & Dubi, Y. Spinterface origin for the chirality-induced spin-selectivity effect. *J. Am. Chem. Soc.* **143**, 14235–14241 (2021).
42. Coropceanu, V. et al. Charge transport in organic semiconductors. *Chem. Rev.* **107**, 926–952 (2007).
43. Kaake, L. G., Barbara, P. F. & Zhu, X.-Y. Intrinsic charge trapping in organic and polymeric semiconductors: A physical chemistry perspective. *J. Phys. Chem. Lett.* **1**, 628–635 (2010).
44. Haneef, H. F., Zeidell, A. M. & Jurchescu, O. D. Charge carrier traps in organic semiconductors: a review on the underlying physics and impact on electronic devices. *J. Mater. Chem. C* **8**, 759–787 (2019).
45. Sachnik, O. et al. Elimination of charge-carrier trapping by molecular design. *Nat. Mater.* **22**, 1114–1120 (2023).
46. Novembre, C., Guérin, D., Lmimouni, K., Gamrat, C. & Vuillaume, D. Gold nanoparticle-pentacene memory transistors. *Appl. Phys. Lett.* **92**, 103314 (2008).
47. Son, D. I., You, C. H., Kim, W. T., Jung, J. H. & Kim, T. W. Electrical bistabilities and memory mechanisms of organic bistable devices based on colloidal ZnO quantum dot-polymethylmethacrylate polymer nanocomposites. *Appl. Phys. Lett.* **94**, 132103 (2009).
48. Burgt, Yvd, Melianas, A., Keene, S. T., Malliaras, G. & Salleo, A. Organic electronics for neuromorphic computing. *Nat. Electron.* **1**, 386–397 (2018).
49. Park, J. et al. Controlled hysteresis of conductance in molecular tunneling junctions. *ACS Nano* **16**, 4206–4216 (2022).
50. Yao, S. & Wang, Z. Edge states and topological invariants of non-hermitian systems. *Phys. Rev. Lett.* **121**, 086803 (2018).
51. Yokomizo, K. & Murakami, S. Non-bloch band theory of non-hermitian systems. *Phys. Rev. Lett.* **123**, 066404 (2019).
52. Zhang, K., Yang, Z. & Fang, C. Correspondence between winding numbers and skin modes in non-hermitian systems. *Phys. Rev. Lett.* **125**, 126402 (2020).
53. Yi, Y. & Yang, Z. Non-hermitian skin modes induced by on-site dissipations and chiral tunneling effect. *Phys. Rev. Lett.* **125**, 186802 (2020).
54. Okuma, N. & Sato, M. Non-hermitian topological phenomena: A review. *Ann. Rev. Conden. Matter Phys.* **14**, 83–107 (2023).
55. Lin, R., Tai, T., Li, L. & Lee, C. H. Topological non-hermitian skin effect. *Front. Phys.* **18**, 53605 (2023).
56. Kawabata, K., Shiozaki, K., Ueda, M. & Sato, M. Symmetry and topology in non-hermitian physics. *Phys. Rev. X* **9**, 041015 (2019).
57. Xiao, L. et al. Non-Hermitian bulk–boundary correspondence in quantum dynamics. *Nat. Phys.* **16**, 761–766 (2020).

58. Helbig, T. et al. Generalized bulk–boundary correspondence in non-Hermitian topolectrical circuits. *Nat. Phys.* **16**, 747–750 (2020).
59. Ghatak, A., Brandenbourger, M., van Wezel, J. & Coulais, C. Observation of non-Hermitian topology and its bulk–edge correspondence in an active mechanical metamaterial. *Proc. Natl. Acad. Sci.* **117**, 29561–29568 (2020).
60. Ochkan, K. et al. Non-hermitian topology in a multi-terminal quantum hall device. *Nat. Phys.* **20**, 395–401 (2024).
61. Abendroth, J. M. et al. Spin-dependent ionization of chiral molecular films. *J. Am. Chem. Soc.* **141**, 3863–3874 (2019).
62. Ghosh, S. et al. Effect of chiral molecules on the electrons' spin wavefunction at interfaces. *J. Phys. Chem. Lett.* **11**, 1550–1557 (2020).
63. Wu, F. et al. Enantiomer-selective magnetoresistance in chiral gold nanocrystals by magnetic control of surface potentials. Preprint at https://doi.org/10.48550/arXiv.2408.03501 (2024).
64. Verhage, M. et al. Chirality-induced magnetic polarization by charge localization in a chiral supramolecular crystal. *Adv. Mater.* **36**, e2403807 (2024).
65. Banerjee-Ghosh, K. et al. Long-range charge reorganization as an allosteric control signal in proteins. *J. Am. Chem. Soc.* **142**, 20456–20462 (2020).
66. Ghosh, S. et al. Substrates modulate charge-reorganization allosteric effects in protein-protein association. *J. Phys. Chem. Lett.* **12**, 2805–2808 (2021).
67. Naaman, R., Paltiel, Y. & Waldeck, D. H. Chiral induced spin selectivity and its implications for biological functions. *Annu. Rev. Biophys.* **51**, 99–114 (2022).
68. Lu, Y., Joy, M., Bloom, B. P. & Waldeck, D. H. Beyond stereoisomeric effects: Exploring the importance of intermolecular electron spin interactions in biorecognition. *J. Phys. Chem. Lett.* **14**, 7032–7037 (2023).
69. Zuo, L. et al. Mechano-electron spin coupling modulates the reactivity of individual coronazymes. *Preprint at* https://doi.org/10.26434/chemrxiv-2023-tt4bh (2023).
70. Liu, T. & Weiss, P. S. Spin polarization in transport studies of chirality-induced spin selectivity. *ACS Nano* **17**, 19502–19507 (2023).
71. Kawabata, K., Okuma, N. & Sato, M. Non-bloch band theory of non-hermitian hamiltonians in the symplectic class. *Phys. Rev. B* **101**, 195147 (2020).
72. Guo, A.-M. & Sun, Q.-F. Spin-selective transport of electrons in DNA double helix. *Phys. Rev. Lett.* **108**, 218102 (2012).
73. Guo, A.-M. et al. Contact effects in spin transport along double-helical molecules. *Phys. Rev. B* **89**, 205434 (2014).
74. Matityahu, S., Utsumi, Y., Aharony, A., Entin-Wohlman, O. & Balseiro, C. A. Spin-dependent transport through a chiral molecule in the presence of spin-orbit interaction and nonunitary effects. *Phys. Rev. B* **93**, 075407 (2016).
75. Piccinin, S., Selloni, A., Scandolo, S., Car, R. & Scoles, G. Electronic properties of metal-molecule-metal systems at zero bias: A periodic density functional study. *J. Chem. Phys.* **119**, 6729–6735 (2003).
76. Souza, Ad. M. et al. Stretching of BDT-gold molecular junctions: thiol or thiolate termination? *Nanoscale* **6**, 14495–14507 (2014).
77. Zhuo, J. et al. Direct spectroscopic evidence for a photodoping mechanism in polythiophene and poly(bithiophene-alt-thienothiophene) organic semiconductor thin films involving oxygen and sorbed moisture. *Adv. Mater.* **21**, 4747–4752 (2009).
78. Nikolka, M. et al. High-mobility, trap-free charge transport in conjugated polymer diodes. *Nat. Commun.* **10**, 2122 (2019).
79. Kotadiya, N. B., Mondal, A., Blom, P. W. M., Andrienko, D. & Wetzelaer, G.-J. A. H. A window to trap-free charge transport in organic semiconducting thin films. *Nat. Mater.* **18**, 1182–1186 (2019).
80. Akkerman, H. B. et al. Electron tunneling through alkanedithiol self-assembled monolayers in large-area molecular junctions. *Proc. Natl. Acad. Sci. USA* **104**, 11161–11166 (2007).
81. Rikken, G. & Avarvari, N. Comparing electrical magnetochiral anisotropy and chirality-induced spin selectivity. *J. Phys. Chem. Lett.* **14**, 9727–9731 (2023).
82. Simmons, J. G. Generalized formula for the electric tunnel effect between similar electrodes separated by a thin insulating film. *J. Appl. Phys.* **34**, 1793–1803 (1963).
83. Naaman, R. & Waldeck, D. H. Spintronics and chirality: Spin selectivity in electron transport through chiral molecules. *Annu. Rev. Phys. Chem.* **66**, 263 – 281 (2015).
84. Julliere, M. Tunneling between ferromagnetic films. *Phys. Lett. A* **54**, 225–226 (1975).
85. Bistritzer, R. & MacDonald, A. H. Moire bands in twisted double-layer graphene. In *Proceedings of the National Academy of Sciences* **108**, (2011).
86. Cao, Y. et al. Correlated insulator behaviour at half-filling in magic-angle graphene superlattices. *Nature* **556**, 80–84 (2018).
87. Cao, Y. et al. Unconventional superconductivity in magic-angle graphene superlattices. *Nature* **556**, 43–50 (2018).
88. Wu, F., Lovorn, T., Tutuc, E., Martin, I. & MacDonald, A. H. Topological insulators in twisted transition metal dichalcogenide homobilayers. *Phys. Rev. Lett.* **122**, 086402 (2019).
89. Zhang, Y., Yuan, N. F. Q. & Fu, L. Moiré quantum chemistry: Charge transfer in transition metal dichalcogenide superlattices. *Phys. Rev. B* **102**, 201115 (2020).
90. Ghiotto, A. et al. Quantum criticality in twisted transition metal dichalcogenides. *Nature* **597**, 345–349 (2021).
91. Xu, Y. et al. A tunable bilayer Hubbard model in twisted WSe2. *Nat. Nanotechnol.* **17**, 934–939 (2022).
92. Wang, C., Gao, Y., Lv, H., Xu, X. & Xiao, D. Stacking domain wall magnons in twisted van der waals magnets. *Phys. Rev. Lett.* **125**, 247201 (2020).
93. Lian, B., Liu, Z., Zhang, Y. & Wang, J. Flat chern band from twisted bilayer $mnbi_2te_4$. *Phys. Rev. Lett.* **124**, 126402 (2020).
94. Kim, J. et al. Observation of plateau-like magnetoresistance in twisted fe3gete2/fe3gete2 junction. *J. Appl. Phys.* **128**, 093901 (2020).
95. Inbar, A. et al. The quantum twisting microscope. *Nature* **614**, 682–687 (2023).
96. Alpern, H. et al. Unconventional superconductivity induced in nb films by adsorbed chiral molecules. *N. J. Phys.* **18**, 113048 (2016).
97. Singh, A. K. et al. Single-molecule junctions map the interplay between electrons and chirality. Preprint at https://doi.org/10.48550/arXiv.2408.12258 (2024).

Acknowledgements

We thank Yossi Paltiel, John M. Abendroth, Tianhan Liu, Peng Xiong, and Paul Weiss for sharing their experimental data and helpful discussions. We are grateful for the inspiring discussions with Yuval Oreg, Eric Akkermans, Ron Naaman, Yizhou Liu, Tobias Holder, ChiYung Yam, Per Hedegard, Oren Tal, D. H. Waldeck, David Mukamel, Oren Raz, Xi Dai, Dali Sun and Zhenfei Liu. B.Y. acknowledges the financial support by the MINERVA Stiftung, the European Research Council (ERC Consolidator Grant "NonlinearTopo", No. 815869), the Minerva Weizmann Programme, and the Israel Science Foundation (ISF, No. 2932/21). K.S. and K.Z. are supported in part by the Office of Naval Research (MURI N00014-20-1-2479).

Author contributions

B.Y. conceived the project and wrote the manuscript with inputs from all authors. Y.Z. and J.X. performed barrier tunneling calculations. K.Z. and K.S. performed non-Hermitian skin effect and two-terminal transmission calculations. All authors analyzed the results.

Competing interests

The authors declare no competing interests.

Additional information

Supplementary information The online version contains supplementary material available at https://doi.org/10.1038/s41467-024-55433-1.

Correspondence and requests for materials should be addressed to Binghai Yan.

Peer review information *Nature Communications* thanks the anonymous reviewers for their contribution to the peer review of this work. A peer review file is available.